catalysts

MDPI

Article

N_8^- Polynitrogen Stabilized on Nitrogen-Doped Carbon Nanotubes as an Efficient Electrocatalyst for Oxygen Reduction Reaction

Zhenhua Yao [1,2], Ruiyang Fan [1], Wangyang Ji [1], Tingxuan Yan [1] and Maocong Hu [1,2,*]

[1] Key Laboratory of Optoelectronic Chemical Materials and Devices, Ministry of Education, School of Chemical and Environmental Engineering, Jianghan University, Wuhan 430056, China; zhenhua.yao@jhun.edu.cn (Z.Y.); fr@stu.jhun.edu.cn (R.F.); 182209101120@stu.jhun.edu.cn (W.J.); tingxuan.yan@stu.jhun.edu.cn (T.Y.)

[2] Department of Chemical and Materials Engineering, New Jersey Institute of Technology, Newark, NJ 07102, USA

* Correspondence: maocong.hu@jhun.edu.cn

Received: 11 July 2020; Accepted: 28 July 2020; Published: 3 August 2020



Abstract: In this work, non-traditional metal-free polynitrogen chain N_8^- deposited on a nitrogen-doped carbon nanotubes (PN-NCNT) catalyst was successfully synthesized by a facile cyclic voltammetry (CV) approach, which was further tested in an oxygen reduction reaction (ORR). The formation of PN on NCNT was confirmed by attenuated total reflectance–Fourier transform infrared spectroscopy (ATR-FTIR) and Raman spectroscopy. Partial positive charge of carbon within NCNT facilitated electron transfer and accordingly induced the formation of more PN species compared to CNT substrate as determined by temperature-programmed decomposition (TPD). Rotating disk electrode (RDE) measurements suggested that a higher current density was achieved over PN-NCNT than that on PN-CNT catalyst, which can be attributed to formation of the larger amount of N_8^- on NCNT. Kinetic study suggested a four-electron pathway mechanism over PN-NCNT. Moreover, it showed long stability and good methanol tolerance, which indicates its great potential application. This work provides insights on designing and synthesizing non-traditional metal-free catalysts for ORR in fuel cells.

Keywords: polynitrogen; metal-free catalyst; oxygen reduction reaction; carbon nanotube

1. Introduction

As an important electrochemical process, the oxygen reduction reaction (ORR) under alkaline conditions has been widely investigated in many applications such as alkaline fuel cells, metal–air batteries, and brine electrolysis [1–4]. The relatively sluggish kinetics of the reaction is regarded as one of the key factors that limits its performance in related applications such as proton exchange membrane fuel cells (PEMFCs) [5–7]. PEMFCs have been considered as one of the most promising future energy conversion devices [8,9], which have attracted much attention from both scientific and industrial views. However, among the factors hampering the widespread application of PEMFCs, are the high-cost and low-performance electrocatalysts, which are responsible for accelerating the sluggish oxygen reduction reaction (ORR) at the cathode, and still need to be improved [10,11]. Pt/C, the current state-of-the-art ORR catalyst, suffers from inherent scarcity, insufficient stability, and high cost [12,13]. Although nonprecious metal catalysts, such as Fe-, Co-, Cu-, and Ni-based materials, can lower the cost, activity and metal leaching are the two major issues to be solved [14–16]. Inspired by the pioneering work from Dai group [17], many studies were conducted to develop metal-free materials as alternative ORR catalysts [18–20]. Most of these types of materials are composed

of heteroatom-doped carbon, which could dramatically reduce the cost as well as increase the efficiency [21–25]. Moreover, the characteristic doping structure prevents active phase leaching [26–29]. However, ORR activity improvement with heteroatom doping is limited since an excessive doped-atom would decrease conductivity of carbon materials [30,31].

A large amount of energy (2.3 eV per atom) is expected to be released upon transforming singly bonded nitrogen to diatomic triply bonded molecular nitrogen [32]. Therefore, polynitrogen compounds have attracted much attention due to their high-energy density while its experimental synthesis is challengeable [33–35]. Molecular N_2 is the only known stable homoatomic nitrogen species before the first synthesis of azide anion N_3^- in 1890, followed by the limited progress on the artificial synthesis of ploynitrogen in the twenty century. It is not until the last decade that several species including N_5^+, N_5^-, N_3, N_4, and cubic gauche (cg) form were experimentally synthesized while extremely rigorous conditions such as high pressure or low temperature were required [36]. Theoretical calculations predicted that charge transfer between a nitrogen chain and carbon nanotube or graphene sheet favored the formation of a polymeric nitrogen chain N_8 [37–39]. Inspired by these theoretical studies, in our previous work, we successfully synthesized negative charged polynitrogen chain phase N_8^- (*abbr.* PN) using cyclic voltammetry (CV) approach with multi-walled carbon nanotubes (MWNTS) [36] and boron-doped graphene (BG) [40] as substrates, respectively. In the very pioneering work, the characterizations results including Fourier transform infrared spectroscopy (FTIR), Raman spectroscopy, and temperature-programmed decomposition (TPD) confirmed the presence of N_8^- on MWNTS. The N_8^- vibrational frequencies data from FTIR and Raman were consistent with DFT calculation results [36]. Furthermore, PN was employed as a catalyst for ORR, which illustrated superior performance while the activity is highly related with the amount of PN species [36]. In the following work, boron-doped graphene (BG) synthesized under hydrothermal conditions was used as the substrate while the same electrochemical synthesis procedure from MWNTS one was followed. Characterization results confirmed the harvest of PN over BG while the PN amount is much larger than that over graphene. It confirmed the assumption that generation of partial positive charge resulted into enhanced electron transfer ability, which would induce the formation of more negative charged N_8^- species [36,40]. Kinetic study was further conducted to investigate the reaction mechanism over PN/BG for oxygen reduction reaction, which indicated a four-electron process [40]. Natural bonding orbital (NBO) analysis was also employed to propose a parallel diatomic adsorption model of O_2 chemisorption over PN (side-on adsorption, Yeager model) [40]. These results inspired us to use other carbon-based materials as the substrate to synthesize large amount of PN for the oxygen reduction reaction application.

In this work, nitrogen-doped carbon nanotube (NCNT) was selected as the substrate to synthesize polynitrogen N_8^- species using cyclic voltammetry (CV) approach under ambient condition. NCNT was selected due to the fact that the higher electronegativity of nitrogen (3.04) than carbon (2.55) would lead to the generation of partial positive charge, which further facilitates the formation of larger amount of PN as concluded by our previous work [40]. Raman and FTIR were used to confirm the harvest of PN species. Temperature Programmed Decomposition (TPD) was employed to investigate the thermal stability and determine the amount of synthesized PN. The PN samples were further used as cathode catalysts for oxygen reduction reaction (ORR) in alkaline condition. Kinetic study indicated a four-electron pathway with high activity. This work provides insights on designing and synthesizing non-traditional metal-free catalysts for ORR in fuel cells.

2. Results and Discussion

The formation of PN on NCNT (or CNT) sheets after CV process was first investigated by ATR-FTIR while the results were demonstrated in Figure 1a. No obvious peak was observed on CNT indicating the characteristic spectra for pristine CNT. Very similar spectra were also obtained on NCNT sample since infrared spectroscopy is insensitive for the low concentration nitrogen doping. FTIR spectra of NaN_3/NCNT sheet and NaN_3/CNT sheet showed the characteristic peak at 2100 cm^{-1},

assigned to the asymmetric stretching mode of azide ion. PN-NCNT and PN-CNT sheet exhibited completely different signals at 2050 cm^{-1}, which can be attributed to polynitrogen chain N_8^- [36,40]. It suggests that PN was successfully synthesized after electrochemical treatment.

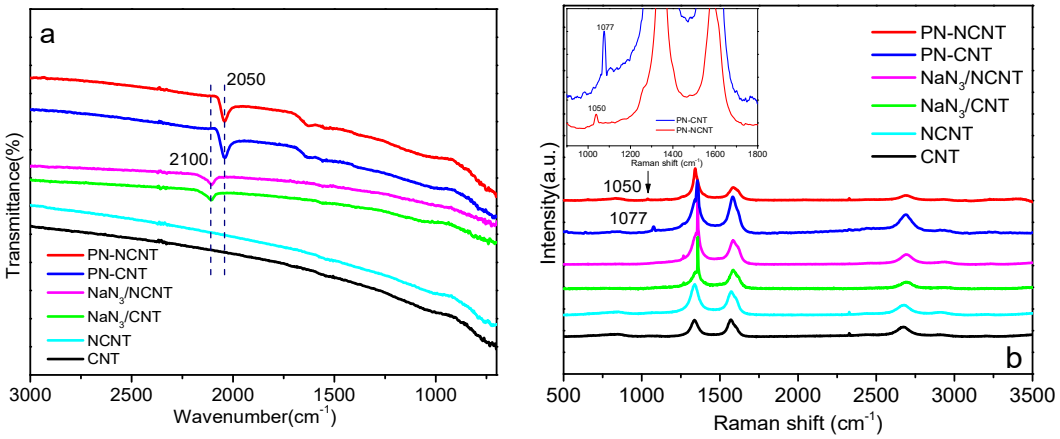

Figure 1. (**a**) ATR-FTIR and (**b**) Raman spectra of CNT, NCNT, NaN_3/CNT, NaN_3/NCNT, PN-CNT, and PN-NCNT (see 3. Materials and Methods for abbreviations).

To further investigate the structures of different samples, Raman spectroscopy was employed while the achieved spectra was illustrated in Figure 1b. It clearly showed that two prominent peaks, namely D-band (~1350 cm^{-1}) and G-band (~1590 cm^{-1}), were observed on all samples [41]. The D-band (disordered band) can be ascribed to the breathing mode of sp^2 rings from the sp^3 defect sites and arises due to defect/disorder present in the graphitic materials [42]. The G band was attributed to active in-plane atomic displacement E2g mode [43]. Moreover, the peak intensity ratio of D over G band (I_D/I_G) can be used as the "sign" of the defect level within CNT [44]. The value of I_D/I_G over CNT is estimated to be 0.98 while that of NCNT is about 1.3. It indicates the increased disorder level of NCNT compared to CNT [45], which can be attributed to the nitrogen doping in the matrix of graphitic structure. However, the presence of the peak around 2700 cm^{-1} in 2D position over NCNT sample suggests the long-range ordering of graphitic structure. For NaN_3/CNT sample, the sharp peak around 1360 cm^{-1} associated with sodium azide overlaps with the carbon nanotube D (defect) mode [32], which is also observed on NaN_3/NCNT. Interestingly, the spectrum of PN-CNT sheet clearly depicts a line at 1077 cm^{-1}, other than those from CNT. It is very close to the characteristic value for PN reported in the previous work (1080 cm^{-1}) indicating the formation of PN [36]. A slight shift was observed over PN-NCNT sheet sample (with line from 1077 to 1050 cm^{-1}), which may be ascribed to the contribution of doped nitrogen, still confirming the generation of PN over NCNT. The morphology of PN species was characterized by TEM as illustrated in Figure 2a. It clearly showed that PN species deposited on the outer-, intra-, and inter-layers of the nanotubes [32,36].

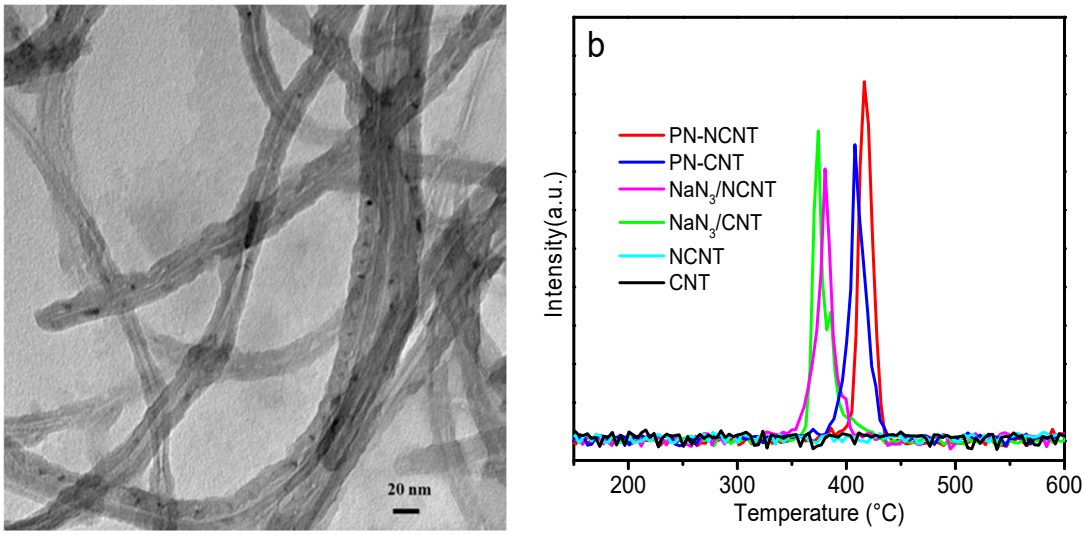

(**a**) (**b**)

Figure 2. (**a**) TEM image of PN-NCNT and (**b**) N^{14} signal from TPD scans of CNT, NCNT, NaN_3/CNT, NaN_3/NCNT, PN-CNT, and PN-NCNT, respectively. The curves were normalized by sample weight (see 3. Materials and Methods for abbreviations).

To investigate the thermal stability and quantify the amount of the synthesized PN species, temperature-programmed decomposition (TPD) was performed over different samples as displayed in Figure 2b. No nitrogen desorption was observed over NCNT sample until 600 °C, which can be attributed to the high stability of incorporated nitrogen within NCNT [46]. The peaks of samples NaN_3/NCNT sheet and NaN_3/CNT sheet locate in the range of 370–380 °C, which can be attributed to the decomposition of sodium azide [40]. In contrast, polynitrogen species N_8^- (in samples PN-NCNT and PN-CNT sheet) are more thermally stable than NaN_3 ones, while decomposition peaks of PN-NCNT and PN-CNT centered at 400–420 °C. Moreover, to quantify the nitrogen amount of each sample, the calibration line was firstly obtained by injecting a series of known amount N_2 into the TPD system. Then after each TPD experiment we integrated the peak area of each sample and compared it with the calibration line to estimate the nitrogen amount as shown in Table 1. Much less nitrogen amount was observed over both NaN_3 samples (0.81 and 0.93 mmol/grams sample) compared to that from two PN samples (1.01 and 1.25 mmol/grams sample). Moreover, it indicated that the amount of N_8^- obtained over PN-NCNT is about 25% more than that of PN-CNT (1.25 vs. 1.01 mmol/grams sample). Due to the higher electronegativity of nitrogen (3.04) than that of carbon (2.55), it may be concluded that positively charged carbon would be created as a result of electron clouds shifting from carbon to nitrogen over NCNT. As indicated by the previous work, partial positive charge would facilitate electron transfer and accordingly induce the formation of more PN species [36,40].

Table 1. Nitrogen amount of each sample (mmol/grams of sample).

Experiment	Sample	Nitrogen Amount [a]
1	NCNT sheet	0
2	CNT sheet	0
3	PN-NCNT sheet	1.25
4	PN-CNT sheet	1.01
5	NaN_3/NCNT sheet	0.81
6	NaN_3/CNT sheet	0.93

[a] Estimated by comparing the peak areas with the standard cure, which was derived via internal standard method by injecting pure nitrogen under the same experimental conditions with TPD.

The electrocatalytic performance of PN-NCNT-GCE and PN-CNT-GCE electrode in oxygen reduction reaction was investigated by LSV measurements. O_2-saturated 0.1 M KOH was the electrolyte. Prior to each measurement, background voltammogram was obtained by carrying out the LSV in a N_2-saturated electrolyte, which was subtracted from the value as measured in O_2-saturated electrolyte. The ORR polarization curves achieved at different rotating speeds were illustrated in Figure 3a (PN-NCNT) and Figure S1a–d (PN-CNT, NCNT, N_3^-/NCNT, and CNT). As expected, current density increased with the electrode rotating speed increase, which can be attributed to the enhanced diffusion of electrolytes [47,48].

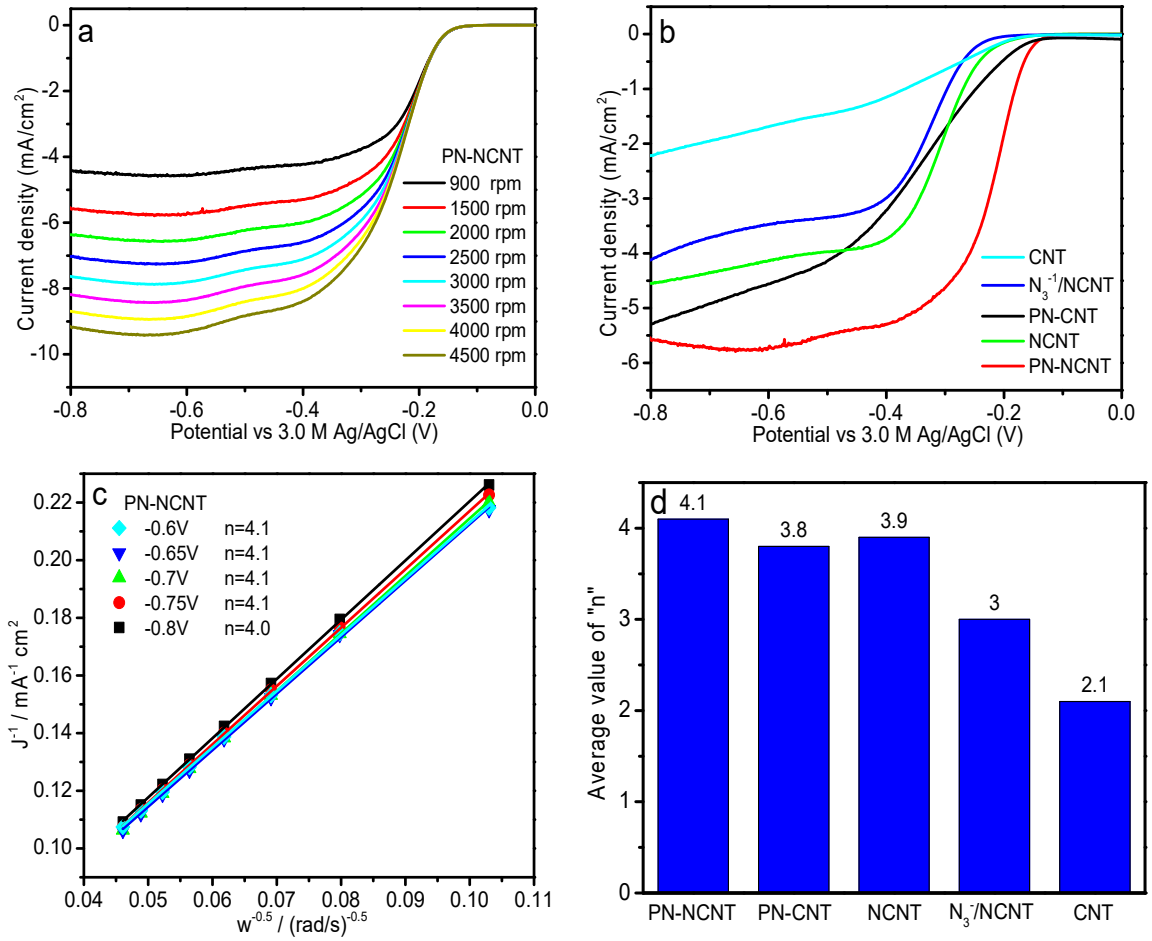

Figure 3. (**a**) LSV curves of PN-NCNT using oxygen-saturated 0.1 M KOH solution as electrolyte at scan rate of 5 mV/s. (**b**) LSV curves of PN-NCNT, PN-CNT, NCNT, N_3^-/NCNT, and CNT using oxygen-saturated 0.1 M KOH solution as electrolyte with rotation speed of 1500 rpm at scan rate of 5 mV/s. (**c**) K-L plots of PN-NCNT at different potentials. (**d**) Average electron transfer number n of PN-NCNT, PN-CNT, NCNT, N_3^-/NCNT, and CNT calculated from K-L equation.

We further compared the current density with a certain rotation speed of 1500 rpm at scan rate of 5 mV/s for all samples. A general trend of PN-NCNT > PN-CNT > NCNT > N_3^-/NCNT > CNT was observed (Figure 3b). Nitrogen-doped carbon nanotubes were widely accepted as superior catalysts for ORR, compared to pristine CNT [49,50], which is also true in our case. With sodium azide dipping, N_3^-/NCNT showed lower current density than NCNT due to the partial coverage of N_3^- over NCNT. Two PN samples (PN-NCNT and PN-CNT) demonstrated much higher current density than NCNT. In consideration of the inferior performance of CNT, it may be concluded that the improved activity of PN samples originated from the highly active PN. Moreover, it is worth mentioning that the PN-NCNT showed the higher current density than PN-CNT. The current density sequence of PN ones is consistent

with that of PN amounts determined in above TPD measurements. The same trend was also reported in our previous study, which was ascribed to the relationship between ORR activity and the amount of PN formed on the substrates [40]. Positively charged carbon of NCNT induced the generation of more PN than that over CNT, which is responsible for higher activity of PN-NCNT compared to PN-CNT.

To further investigate the enhanced mechanism, Koutecky-Levich (K-L) equation listed below was used to evaluate the kinetics of the ORR process in this work [51,52]:

$$\frac{1}{J} = \frac{1}{J_L} + \frac{1}{J_k} = \frac{1}{B\omega^{0.5}} + \frac{1}{J_k} \quad (1)$$

$$B = 0.62nFC_o(D_o)^{2/3}\nu^{-1/6} \quad (2)$$

where J in Equation (1) is the measured current density, J_L and J_k in Equation (1) are the diffusion and kinetic limiting current density, respectively. B is the Levich constant, ω in Equation (1) is the angular velocity (rad s^{-1}), n in Equation (2) is the transferred electron number per oxygen molecule for the reaction, F in Equation (2) is the Faraday constant with the value of 96,485 C cm^{-1}, C_o in Equation (2) is the bulk concentration of O_2 with the value of 1.2×10^{-3} mol L^{-1}, D_o in Equation (2) is the diffusion coefficient of O_2 with the value of 1.9×10^{-5} cm s^{-1}, ν in Equation (2) is the kinematic viscosity of the electrolyte with the value of 0.01 cm^2 s^{-1}. The K-L plots of $1/J$ vs. $1/\omega^{0.5}$ for all five samples were illustrated in Figure 3c (PN-NCNT) and Figure S2a–d (PN-CNT, NCNT, N_3^-/NCNT, and CNT). Well-linear and parallel lines was achieved for all the samples after fitting, indicating a first-order reaction toward dissolved oxygen [53,54]. Average electron transfer number n of all five samples was further achieved from slopes of K-L plots as shown in Figure 3d [19]. The n value of 2.1 was derived from the CNT electrode, which indicated a typical two-electron process over CNT [17]. In contrast, NCNT displayed a dominant four-electron pathway with n value of 3.9, which is consistent with the literatures [55–57]. With sodium azide dipping, the n value for N_3^-/NCNT was 3, indicating a coexisting pathway involving both the two-electron and four-electron processes [58]. It may be ascribed to the partial coverage of N_3^-, which is through a two-electron pathway [36,40], over NCNT. Both PN-NCNT and PN-CNT demonstrated a four-electron process based on the derived electron transfer number n (4.1 and 3.8, respectively). In consideration of the two-electron pathway over CNT as revealed before, it clearly indicates a four-electron mechanism on PN, which is consistent with our previous work [36,40]. Based on the previous calculation results [36,40], there're two most active sites within the polynitrogen chain N_8^-: adjacent N1 and N2 locating in the center of the polynitrogen chain. These two nitrogen atoms have more negative charges than other six ones (as shown in Figure S3). Direct bonding with N1 and N2 atoms would activate oxygen molecules as demonstrated in our previous work and other study [36,59,60], i.e., side-on adsorption of oxygen with the two adjacent active sites (N1 and N2 in this work) (Yeager model [17]). The relatively stable O-O bond would then be effectively weakened and further easily broken [40]. As a result, four-electron transfer process would take place during oxygen reduction [61,62] as observed in the above kinetic study for PN samples. In contrast, azide is a linear centrosymmetric anion, while two end nitrogen atoms have more negative charges than the center one [63,64]. Therefore, it's reasonable to assume that oxygen molecules would be chemisorbed on the end nitrogen atoms via an end-on adsorption (i.e., Pauling model [60]). As a result, two-electron transfer pathway would rule the reaction for oxygen reduction [61,62], as concluded in the previous work [40].

We further evaluated the long-term stability of PN-NCNT catalysts using a chronoamperometric method (Figure 4a). A negligible decrease (~3.1%) was observed over PN-NCNT while almost 14.4% loss was detected on Pt/C catalyst, suggesting the much better stability of PN-NCNT. It can be attributed to the strong interactions between negatively charged polynitrogen chain phase N_8^- and positively charged carbon of NCNT substrate. Methanol crossover effect was further tested. 0.5 M methanol was injected into an oxygen-saturated 0.1 M KOH solution at a certain time during a chronoamperometric measurement. No obvious disturbance of the current was observed over PN-NCNT while sharp

decrease occurred on Pt/C (Figure 4b), which indicated the superior methanol tolerance of PN-NCNT compared to Pt/C. These results together with the high activity suggest that PN-NCNT is a potential metal-free catalyst for oxygen reduction reaction in fuel cell application.

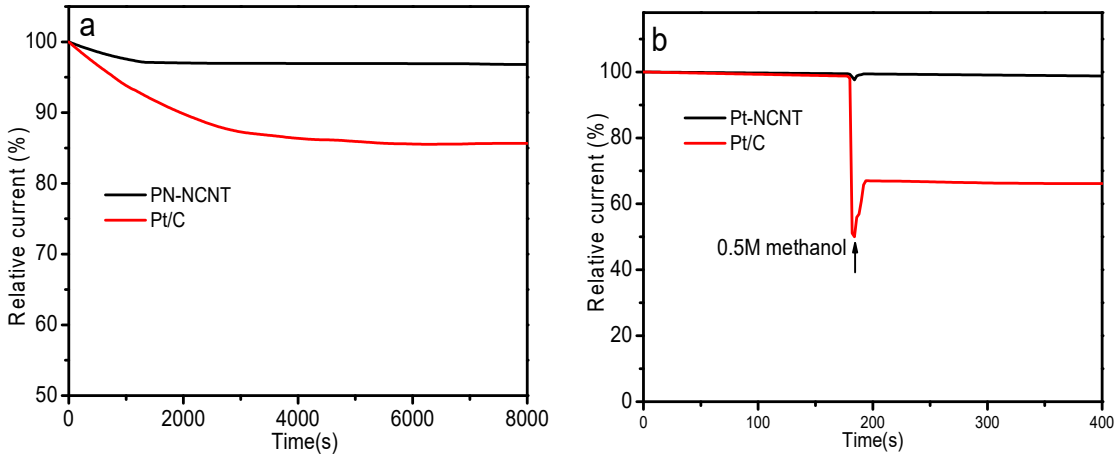

Figure 4. (**a**) Long-term test of PN-NCNT and Pt/C while an oxygen-saturated 0.1 M KOH solution was employed as the electrolyte as well as the rotation speed setting at 1500 rpm. (**b**) Methanol tolerance of PN-NCNT and Pt/C, while an oxygen-saturated 0.1 M KOH solution was employed as the electrolyte as well as the rotation speed setting at 1500 rpm with the injection of 0.5 M methanol during a chronoamperometric measurement.

3. Materials and Methods

Nitrogen-doped multi-wall carbon nanotubes (NCNT) and multi-wall carbon nanotubes (CNT) were purchased from Cheaptubes. Polynitrogen N_8^- was prepared using computer-controlled CH Instruments 760 in a three-electrode setup, which followed previous work [36,40] while using NCNT instead of MWNTS or graphene as substrates. Briefly, 10 mg NCNT powder was ultrasonically dispersed into 5 mL ethanol containing a Nafion solution (0.5 wt%, DuPont). 5 µL of the prepared ink was then coated onto the surface of a pre-polished glassy carbon electrode (*abbr.* GCE, with diameter of 3.0 mm) and further dried in air overnight. It was denoted as NCNT-GCE, which was used as the working electrode. Control experiment over CNT was also conducted while CNT-GCE electrode was achieved. The counter and reference electrode were Pt and Ag/AgCl, respectively. 2 M NaN_3-buffer solution (with PH value of 4.0) was employed as electrolyte. The CV scan cycle was set to be 12 with scan rate of 1 mV/s while the potential range is between +0.8V and −0.8V. The resulting sample was then dried overnight in the air, denoting as PN-NCNT-GCE and PN-CNT-GCE electrode, respectively. Both were further employed as the working electrodes in the following ORR test.

The rotating disk electrode (RDE) system (ALS Co., Ltd., Tokyo, Japan) was employed to perform ORR tests while linear sweep voltammetry (LSV) measurements was carried out. The scanning rate is set as 5 mV/s while various rotating speeds were used. PN-NCNT-GCE (or PN-CNT-GCE) were the working electrodes. The counter and reference electrode were Pt and Ag/AgCl, respectively. The electrolyte is 0.1 M KOH solution. To saturate the electrolyte, oxygen (or nitrogen) was continuously bubbled into the system for at least 30 min prior to the experiments. Moreover, to maintain saturation, oxygen (or nitrogen) was also flowed into the system during the experiments. Control experiment over 20 wt.% Pt/C was also performed [17].

For characterizations purpose, large amount of PN were synthesized using round-shaped NCNT (or CNT) sheets (labelled as PN-NCNT and PN-CNT sheet), instead of GCE ones (NCNT-GCE or CNT-GCE), as substrates (working electrodes). The sheets were fabricated by vacuum filtration of NCNT (or CNT) dispersion following the procedures in the previous work [36,40]. Two control experiments were also performed by dipping NCNT (or CNT) sheets into 2 M NaN_3-buffer solution

with PH value of 4.0 but without electrochemical process to prepare NaN_3/NCNT sheet (or NaN_3/CNT sheet). Raman spectroscopy was performed with a Thermo Scientific DXR Raman microscope with 532 nm laser excitation at a spectral resolution of 2 cm^{-1} and a spatial resolution of 10 μm. TEM was conducted with a Hitachi H7500 (Japan). FTIR was carried out using a Nicolet ThermoElectron spectrometer combined with a MIRacle ATR platform assembly and a ZnSe plate, and denoted as ATR-FTIR. Temperature programmed decomposition (TPD) was performed using an AutoChem II 2920 system (Micromeritics). Typically, samples were heated in helium flow from room temperature to 600 °C with a heating rate of 10 °C/min while the effluent gas was detected with an on-line mass spectrometer (Agilent 7010A, US).

4. Conclusions

Following our previous observations on PN synthesis and its application in oxygen reduction reactions, in this work, nitrogen-doped carbon nanotubes (NCNTs) were selected as substrates to synthesize a polynitrogen chain N_8^- (PN) catalyst with a cyclic voltammetry (CV) method while the synthesized PN was further tested for ORR. Both ATR-FTIR and Raman spectroscopy confirmed the harvest of PN. TPD results indicated that PN was more thermally stable than sodium azide. Moreover, the quantitative analysis based on TPD determined that a larger amount of PN deposited on NCNT compared to that over CNT. It can be attributed to the formation of partial positive charge of carbon within NCNT, which facilitated electron transfer. Rotating disk electrode (RDE) measurements suggested that higher current density was observed over PN-NCNT than that on PN-CNT, which can be ascribed to the larger amount of PN on NCNT. Kinetic study suggested that PN-NCNT was through a four-electron pathway while the reaction mechanism was revealed. Moreover, it showed long stability and good methanol tolerance, which indicates its great potential application. This work provides a facile strategy to design and synthesize non-traditional metal-free catalysts for ORR in fuel cells.

Supplementary Materials: The following are available online at http://www.mdpi.com/2073-4344/10/8/864/s1, Figure S1: LSV curves of PN-CNT, NCNT, N3−/NCNT, and CNT using oxygen-saturated 0.1 M KOH solution as electrolyte at scan rate of 5 mV/s. Figure S2: The K-L plots of 1/J vs. 1/ ω0.5 for PN-CNT, NCNT, N3−/NCNT, and CNT. Figure S3: NBO calculation results of partial charge distribution on a PN anion.

Author Contributions: Conceptualization, Z.Y. and M.H.; methodology, M.H.; investigation, R.F., W.J., and T.Y.; writing—original draft preparation, Z.Y.; writing—review and editing, M.H.; supervision, M.H.; project administration, M.H.; funding acquisition, Z.Y. and M.H. All authors have read and agreed to the published version of the manuscript.

Funding: The financial support from Jianghan University is greatly appreciated.

Acknowledgments: We appreciated Yan Cai (Hanyang No.1 High School, Caidian District, Wuhan 430100, China) for the valuable discussion on the work.

Conflicts of Interest: The authors declare no conflict of interest.

References

1. Singh, S.K.; Takeyasu, K.; Nakamura, J. Active sites and mechanism of oxygen reduction reaction electrocatalysis on nitrogen-doped carbon materials. *Adv. Mater.* **2019**, *31*, 1804297. [CrossRef] [PubMed]
2. Menshchikov, V.; Alekseenko, A.; Guterman, V.; Nechitailov, A.; Glebova, N.; Tomasov, A.; Spiridonova, O.; Belenov, S.; Zelenina, N.; Safronenko, O. Effective platinum-copper catalysts for methanol oxidation and oxygen reduction in proton-exchange membrane fuel cell. *Nanomaterials* **2020**, *10*, 742. [CrossRef] [PubMed]
3. Yan, T.; Wan, Z.; Wang, K.; Hu, M.; Wang, X. A 3D carbon foam derived from phenol resin via cscl soft-templating approach for high-performance supercapacitor. *Energy Technol.* **2020**, *8*, 1901301. [CrossRef]
4. Cui, C.; Sun, M.; Zhu, X.; Han, J.; Wang, H.; Ge, Q. Oxygen reduction reaction catalyzed by Pt3M (M = 3d Transition Metals) supported on o-doped graphene. *Catalysts* **2020**, *10*, 156. [CrossRef]
5. Dembinska, B.; Zlotorowicz, A.; Modzelewska, M.; Miecznikowski, K.; Rutkowska, I.A.; Stobinski, L.; Malolepszy, A.; Krzywiecki, M.; Zak, J.; Negro, E.; et al. Low-noble-metal-loading hybrid catalytic system for oxygen reduction utilizing reduced-graphene-oxide-supported platinum aligned with carbon-nanotube-supported iridium. *Catalysts* **2020**, *10*, 689. [CrossRef]

6. Rivera, L.M.; Fajardo, S.; Arévalo, M.D.C.; García, G.; Pastor, E. S- and N-doped graphene nanomaterials for the oxygen reduction reaction. *Catalysts* **2017**, *7*, 278. [CrossRef]
7. Song, M.; Song, Y.; Sha, W.; Xu, B.; Guo, J.; Wu, Y. Recent advances in non-precious transition metal/nitrogen-doped carbon for oxygen reduction electrocatalysts in PEMFCs. *Catalysts* **2020**, *10*, 141. [CrossRef]
8. Liu, X.-M.; Cui, X.; Dastafkan, K.; Wang, H.-F.; Tang, C.; Zhao, C.; Chen, A.; He, C.; Han, M.; Zhang, Q. Recent advances in spinel-type electrocatalysts for bifunctional oxygen reduction and oxygen evolution reactions. *J. Energy Chem.* **2021**, *53*, 290–302. [CrossRef]
9. Li, Y.; Tong, Y.; Peng, F. Metal-free carbocatalysis for electrochemical oxygen reduction reaction: Activity origin and mechanism. *J. Energy Chem.* **2020**, *48*, 308–321. [CrossRef]
10. Antiochia, R.; Oyarzun, D.; Sánchez, J.; Tasca, F. Comparison of direct and mediated electron transfer for bilirubin oxidase from myrothecium verrucaria. effects of inhibitors and temperature on the oxygen reduction reaction. *Catalysts* **2019**, *9*, 1056. [CrossRef]
11. Zhang, Y.-C.; Ullah, S.; Zhang, R.; Pan, L.; Zhang, X.; Zou, J.-J. Manipulating electronic delocalization of Mn3O4 by manganese defects for oxygen reduction reaction. *Appl. Catal. B Environ.* **2020**, *277*, 119247. [CrossRef]
12. Kim, Y.; Jeffery, A.A.; Min, J.; Jung, N. Modulating catalytic activity and durability of ptfe alloy catalysts for oxygen reduction reaction through controlled carbon shell formation. *Nanomaterials* **2019**, *9*, 1491. [CrossRef] [PubMed]
13. Zeng, Q.; Zhang, X.; Wang, W.; Zhang, D.; Jiang, Y.; Zhou, X.; Lin, B. A Zn-Doped Ba0.5Sr0.5Co0.8Fe0.2O3-δ perovskite cathode with enhanced orr catalytic activity for SOFCs. *Catalysts* **2020**, *10*, 235. [CrossRef]
14. Luque-Centeno, J.M.; Martínez-Huerta, M.V.; Sebastián, D.; Pardo, J.I.; Lázaro, M.J. CoTiO3/NrGO nanocomposites for oxygen evolution and oxygen reduction reactions: Synthesis and electrocatalytic performance. *Electrochim. Acta* **2020**, *331*, 135396. [CrossRef]
15. Wei, M.; Huang, S.; Wang, Y.; Liu, Y.; He, Y.; Wang, C.; Yang, L. Nanostructured Ru-doped Co3O4 as an efficient electrocatalyst for oxygen reduction reaction in alkaline medium. *J. Alloy. Compd.* **2020**, *827*, 154207. [CrossRef]
16. Cui, X.; Meng, L.; Zhang, X.; Wang, X.; Shi, J. Heterogeneous atoms-doped titanium carbide as a precious metal-free electrocatalyst for oxygen reduction reaction. *Electrochim. Acta* **2019**, *295*, 384–392. [CrossRef]
17. Gong, K.; Du, F.; Xia, Z.; Durstock, M.; Dai, L. Nitrogen-doped carbon nanotube arrays with high electrocatalytic activity for oxygen reduction. *Science* **2009**, *323*, 760. [CrossRef]
18. Liu, Y.; Liu, Z.; Liu, H.; Liao, M. Novel porous nitrogen doped graphene/carbon black composites as efficient oxygen reduction reaction electrocatalyst for power generation in microbial fuel cell. *Nanomaterials* **2019**, *9*, 836. [CrossRef]
19. Dahal, B.; Chae, S.-H.; Muthurasu, A.; Mukhiya, T.; Gautam, J.; Chhetri, K.; Subedi, S.; Ojha, G.P.; Tiwari, A.P.; Lee, J.H.; et al. An innovative synthetic approach for core-shell multiscale hierarchically porous boron and nitrogen codoped carbon nanofibers for the oxygen reduction reaction. *J. Power Sources* **2020**, *453*, 227883. [CrossRef]
20. Li, Y.; Mo, C.; Li, J.; Yu, D. Pyrazine–nitrogen–rich exfoliated C4N nanosheets as efficient metal–free polymeric catalysts for oxygen reduction reaction. *J. Energy Chem.* **2020**, *49*, 243–247. [CrossRef]
21. Liang, Z.; Fan, X.; Lei, H.; Qi, J.; Li, Y.; Gao, J.; Huo, M.; Yuan, H.; Zhang, W.; Lin, H.; et al. Cobalt–nitrogen-doped helical carbonaceous nanotubes as a class of efficient electrocatalysts for the oxygen reduction reaction. *Angew. Chem. Int. Ed.* **2018**, *57*, 13187–13191. [CrossRef] [PubMed]
22. Ren, S.-B.; Chen, X.-L.; Li, P.-X.; Hu, D.-Y.; Liu, H.-L.; Chen, W.; Xie, W.-B.; Chen, Y.; Yang, X.-L.; Han, D.-M.; et al. Nitrogen and sulfur dual-doped carbon nanotube derived from a thiazolothiazole based conjugated microporous polymer as efficient metal-free electrocatalysts for oxygen reduction reaction. *J. Power Sources* **2020**, *461*, 228145. [CrossRef]
23. Pepè Sciarria, T.; de Oliveira, M.A.C.; Mecheri, B.; D'Epifanio, A.; Goldfarb, J.L.; Adani, F. Metal-free activated biochar as an oxygen reduction reaction catalyst in single chamber microbial fuel cells. *J. Power Sources* **2020**, *462*, 228183. [CrossRef]
24. Tran, T.Q.; Lee, J.K.Y.; Chinnappan, A.; Loc, N.H.; Tran, L.T.; Ji, D.; Jayathilaka, W.A.D.M.; Kumar, V.V.; Ramakrishna, S. High-performance carbon fiber/gold/copper composite wires for lightweight electrical cables. *J. Mater. Sci. Technol.* **2020**, *42*, 46–53. [CrossRef]

25. Wang, L.; Dou, S.; Xu, J.; Liu, H.K.; Wang, S.; Ma, J.; Dou, S.X. Highly nitrogen doped carbon nanosheets as an efficient electrocatalyst for the oxygen reduction reaction. *Chem. Commun.* **2015**, *51*, 11791–11794. [CrossRef] [PubMed]
26. Marbaniang, P.; Ingavale, S.; Catherin, D.; Ramgir, N.; Swami, A.; Kakade, B. Forming a BB bond in boron carbon nitride composite: A way for metal free electrocatalyst for oxygen reduction reaction in alkaline medium. *J. Catal.* **2019**, *378*, 104–112. [CrossRef]
27. Yang, J.; Xiang, F.; Guo, H.; Wang, L.; Niu, X. Honeycomb-like porous carbon with N and S dual-doping as metal-free catalyst for the oxygen reduction reaction. *Carbon* **2020**, *156*, 514–522. [CrossRef]
28. Wang, Z.; Wu, H.-H.; Li, Q.; Besenbacher, F.; Li, Y.; Zeng, X.C.; Dong, M. reversing interfacial catalysis of ambipolar WSe2 single crystal. *Adv. Sci.* **2020**, *7*, 1901382. [CrossRef]
29. Wang, Z.; Liu, J.; Hao, X.; Wang, Y.; Chen, Y.; Li, P.; Dong, M. Enhanced power density of supercapacitor by introducing 3D-interfacial graphene. *New J. Chem.* **2020**. [CrossRef]
30. Hu, M.; Yao, Z.; Wang, X. Characterization techniques for graphene-based materials in catalysis. *AIMS Mater. Sci.* **2017**, *4*, 755–788. [CrossRef]
31. Hu, M.; Yao, Z.; Wang, X. Graphene-based nanomaterials for catalysis. *Ind. Eng. Chem. Res.* **2017**, *56*, 3477–3502. [CrossRef]
32. Benchafia, E.M.; Yao, Z.; Yuan, G.; Chou, T.; Piao, H.; Wang, X.; Iqbal, Z. Cubic gauche polymeric nitrogen under ambient conditions. *Nat. Commun.* **2017**, *8*, 930. [CrossRef] [PubMed]
33. Uddin, J.; Barone, V.; Scuseria, G.E. Energy storage capacity of polymeric nitrogen. *Mol. Phys.* **2006**, *104*, 745–749. [CrossRef]
34. Peng, F.; Yao, Y.; Liu, H.; Ma, Y. Crystalline LiN5 predicted from first-principles as a possible high-energy material. *J. Phys. Chem. Lett.* **2015**, *6*, 2363–2366. [CrossRef]
35. Eremets, M.I.; Gavriliuk, A.G.; Trojan, I.A.; Dzivenko, D.A.; Boehler, R. Single-bonded cubic form of nitrogen. *Nat. Mater.* **2004**, *3*, 558–563. [CrossRef]
36. Wu, Z.; Benchafia, E.M.; Iqbal, Z.; Wang, X. N8 polynitrogen stabilized on multi-wall carbon nanotubes for oxygen-reduction reactions at ambient conditions. *Angew. Chem. Int. Ed.* **2014**, *53*, 12555–12559. [CrossRef]
37. Abou-Rachid, H.; Hu, A.; Timoshevskii, V.; Song, Y.; Lussier, L.S. Nanoscale high energetic materials: A polymeric nitrogen chain N8 confined inside a carbon nanotube. *Phys. Rev. Lett.* **2008**, *100*, 196401. [CrossRef]
38. Ji, W.; Timoshevskii, V.; Guo, H.; Abou-Rachid, H.; Lussier, L. Thermal stability and formation barrier of a high-energetic material N 8 polymer nitrogen encapsulated in (5,5) carbon nanotube. *Appl. Phys. Lett.* **2009**, *95*, 012904. [CrossRef]
39. Timoshevskii, V.; Ji, W.; Abou-Rachid, H.; Lussier, L.S.; Guo, H. Polymeric nitrogen in a graphene matrix: An ab initio study. *Phys. Rev. B Condens. Matter Mater. Phys.* **2009**, *80*, 115409. [CrossRef]
40. Yao, Z.; Hu, M.; Iqbal, Z.; Wang, X. N8– polynitrogen stabilized on boron-doped graphene as metal-free electrocatalysts for oxygen reduction reaction. *ACS Catal.* **2020**, *10*, 160–167. [CrossRef]
41. Haque, A.; Sachan, R.; Narayan, J. Synthesis of diamond nanostructures from carbon nanotube and formation of diamond-CNT hybrid structures. *Carbon* **2019**, *150*, 388–395. [CrossRef]
42. Tripathi, P.; Bhatnagar, A.; Ramesh, A.; Vishwakarma, A.K.; Singh, S.; Bailmare, D.B.; Deshmukh, A.D.; Gupta, B.K.; Srivastava, O.N. Radially aligned CNTs derived carbon hollow cylinder architecture for efficient energy storage. *Electrochim. Acta* **2020**, *354*, 136650. [CrossRef]
43. Abitkar, S.B.; Jadhav, P.R.; Tarwal, N.L.; Moholkar, A.V.; Patil, C.E. A facile synthesis of α-Ni(OH)2-CNT composite films for supercapacitor application. *Adv. Powder Technol.* **2019**, *30*, 2285–2292. [CrossRef]
44. Zeng, X.; Wang, Z.; Meng, N.; McCarthy, D.T.; Deletic, A.; Pan, J.-h.; Zhang, X. Highly dispersed TiO2 nanocrystals and carbon dots on reduced graphene oxide: Ternary nanocomposites for accelerated photocatalytic water disinfection. *Appl. Catal. B* **2017**, *202*, 33–41. [CrossRef]
45. Salinas-Torres, D.; Navlani-García, M.; Mori, K.; Kuwahara, Y.; Yamashita, H. Nitrogen-doped carbon materials as a promising platform toward the efficient catalysis for hydrogen generation. *Appl. Catal. A Gen.* **2019**, *571*, 25–41. [CrossRef]
46. Liu, H.; Zhang, Y.; Li, R.; Sun, X.; Abou-Rachid, H. Thermal and chemical durability of nitrogen-doped carbon nanotubes. *J. Nanopart. Res.* **2012**, *14*, 1016. [CrossRef]

47. Jin, H.; Huang, H.; He, Y.; Feng, X.; Wang, S.; Dai, L.; Wang, J. Graphene quantum dots supported by graphene nanoribbons with ultrahigh electrocatalytic performance for oxygen reduction. *J. Am. Chem. Soc.* **2015**, *137*, 7588–7591. [CrossRef]
48. Wang, W.; Chen, J.-Q.; Tao, Y.-R.; Zhu, S.-N.; Zhang, Y.-X.; Wu, X.-C. Flowerlike Ag-Supported Ce-Doped Mn3O4 nanosheet heterostructure for a highly efficient oxygen reduction reaction: Roles of metal oxides in Ag surface states. *ACS Catal.* **2019**, *9*, 3498–3510. [CrossRef]
49. Niu, W.-J.; Wang, Y.-P.; He, J.-Z.; Liu, W.-W.; Liu, M.-C.; Shan, D.; Lee, L.; Chueh, Y.-L. Highly stable nitrogen-doped carbon nanotubes derived from carbon dots and metal-organic frameworks toward excellent efficient electrocatalyst for oxygen reduction reaction. *Nano Energy* **2019**, *63*, 103788. [CrossRef]
50. Deng, H.; Li, Q.; Liu, J.; Wang, F. Active sites for oxygen reduction reaction on nitrogen-doped carbon nanotubes derived from polyaniline. *Carbon* **2017**, *112*, 219–229. [CrossRef]
51. Lai, L.; Potts, J.R.; Zhan, D.; Wang, L.; Poh, C.K.; Tang, C.; Gong, H.; Shen, Z.; Lin, J.; Ruoff, R.S. Exploration of the active center structure of nitrogen-doped graphene-based catalysts for oxygen reduction reaction. *Energy Environ. Sci.* **2012**, *5*, 7936–7942. [CrossRef]
52. Selvakumar, K.; Senthil Kumar, S.M.; Thangamuthu, R.; Ganesan, K.; Murugan, P.; Rajput, P.; Jha, S.N.; Bhattacharyya, D. Physiochemical Investigation of Shape-Designed MnO2 Nanostructures and Their Influence on Oxygen Reduction Reaction Activity in Alkaline Solution. *J. Phys. Chem. C* **2015**, *119*, 6604–6618. [CrossRef]
53. Li, Y.; Zhao, Y.; Cheng, H.; Hu, Y.; Shi, G.; Dai, L.; Qu, L. Nitrogen-doped graphene quantum dots with oxygen-rich functional groups. *J. Am. Chem. Soc.* **2012**, *134*, 15–18. [CrossRef] [PubMed]
54. Wang, Y.; Liu, H.; Wang, K.; Song, S.; Tsiakaras, P. 3D interconnected hierarchically porous N-doped carbon with NH3 activation for efficient oxygen reduction reaction. *Appl. Catal. B Environ.* **2017**, *210*, 57–66. [CrossRef]
55. Yang, L.; Shui, J.; Du, L.; Shao, Y.; Liu, J.; Dai, L.; Hu, Z. Carbon-based metal-free ORR Electrocatalysts for fuel cells: Past, present, and future. *Adv. Mater.* **2019**, *31*, 1804799. [CrossRef] [PubMed]
56. Quílez-Bermejo, J.; Morallón, E.; Cazorla-Amorós, D. Metal-free heteroatom-doped carbon-based catalysts for ORR: A critical assessment about the role of heteroatoms. *Carbon* **2020**, *165*, 434–454. [CrossRef]
57. Dai, L.; Xue, Y.; Qu, L.; Choi, H.-J.; Baek, J.-B. Metal-free catalysts for oxygen reduction reaction. *Chem. Rev.* **2015**, *115*, 4823–4892. [CrossRef]
58. Wang, S.; Yu, D.; Dai, L. Polyelectrolyte functionalized carbon nanotubes as efficient metal-free electrocatalysts for oxygen reduction. *J. Am. Chem. Soc.* **2011**, *133*, 5182–5185. [CrossRef]
59. Deng, D.; Pan, X.; Yu, L.; Cui, Y.; Jiang, Y.; Qi, J.; Li, W.-X.; Fu, Q.; Ma, X.; Xue, Q.; et al. Toward N-Doped graphene via solvothermal synthesis. *Chem. Mater.* **2011**, *23*, 1188–1193. [CrossRef]
60. Shi, Z.; Zhang, J.; Liu, Z.-S.; Wang, H.; Wilkinson, D.P. Current status of ab initio quantum chemistry study for oxygen electroreduction on fuel cell catalysts. *Electrochim. Acta* **2006**, *51*, 1905–1916. [CrossRef]
61. Zhang, L.; Xia, Z. Mechanisms of oxygen reduction reaction on nitrogen-doped graphene for fuel cells. *J. Phys. Chem. C* **2011**, *115*, 11170–11176. [CrossRef]
62. Chen, R.; Li, H.; Chu, D.; Wang, G. Unraveling oxygen reduction reaction mechanisms on carbon-supported Fe-Phthalocyanine and Co-Phthalocyanine catalysts in alkaline solutions. *J. Phys. Chem. C* **2009**, *113*, 20689–20697. [CrossRef]
63. Stevens, E.D.; Hope, H. A study of the electron-density distribution in sodium azide, NaN3. *Acta Crystallogr. Sect. A* **1977**, *33*, 723–729. [CrossRef]
64. Wang, X.; Li, J.; Zhu, H.; Chen, L.; Lin, H. Polymerization of nitrogen in cesium azide under modest pressure. *J. Chem. Phys.* **2014**, *141*, 044717. [CrossRef] [PubMed]



© 2020 by the authors. Licensee MDPI, Basel, Switzerland. This article is an open access article distributed under the terms and conditions of the Creative Commons Attribution (CC BY) license (http://creativecommons.org/licenses/by/4.0/).